Materials Characterization 170 (2020) 110638

Contents lists available at ScienceDirect

Materials Characterization

journal homepage: www.elsevier.com/locate/matchar

Characterization of the interpass microstructure in low alloy steel/Alloy 625 HW-GTAW narrow groove welds

Ryan Buntain[a,*], Boian Alexandrov[a], Gopal Viswanathan[b]

[a] Welding Engineering Department, The Ohio State University, Columbus, OH, United States
[b] Materials Science and Engineering Department, The Ohio State University, Columbus, OH, United States

ABSTRACT

A dissimilar weld between a low alloy steel (LAS) butter weld joined to a F65 steel pipe using a narrow groove hot wire gas tungsten arc welding (HW-GTAW) procedure with Alloy 625 filler metal was investigated. The weld interpass microstructure is comprised of large swirls formed by a macrosegregation mechanism involving partial, non-uniform mixing of liquid base metal with the lower melting temperature weld pool, followed by fast solidification. This mechanism produces steep gradients in composition and solidification behavior. The resulting swirls are composed of alternating iron-rich peninsulas and partially mixed zones (PMXZ) that are surrounded by planar and cellular zones exhibiting multiple solidification directions. Large austenitic grains, encompassing planar, cellular, and dendritic morphologies, nucleate off peninsulas in direct contact with the weld pool. The highest hardness was found in nickel and chromium rich PMXZs that exhibited a lath martensite microstructure. In the event of exposure to hydrogen containing environments, the PMXZs could serve as nucleation sites for hydrogen assisted cracking.

1. Introduction

The oil and gas industry commonly uses nickel based Alloy 625 to join and clad subsea equipment made of high strength low alloy steel (LAS). Subsea equipment made using these high strength steel grades require a post weld heat treatment (PWHT) after welding to temper the heat affected zone (HAZ) microstructure and relieve residual stress. Performing PWHT on welded structures containing these steels is often not possible. Butter welds can be added to act as a transition joint to eliminate the need for PWHT after welding. A butter weld, traditionally made of Alloy 625, is deposited on a high strength steel forging at a production facility. This assembly is then subjected to PWHT and welded to a steel pipe with an Alloy 625 closure weld either in the production facility or in the field. The new HAZ is contained within the Alloy 625 butter weld rather than the high strength steel forging, thus eliminating the need for a PWHT. A schematic of a traditional Alloy 625 butter weld assembly used for subsea service is shown in Fig. 1a.

There have been multiple failures of Alloy 625 butter welds on high strength steel forgings during subsea service while under cathodic protection [1–4]. These failures were attributed to hydrogen assisted cracking (HAC) due to local saturation with hydrogen of relatively brittle microstructural constituents at the dissimilar interface. The embrittlement mechanism involves formation of fresh martensite along with carbon accumulation and carbide precipitation within the dissimilar transition zone during PWHT. Fresh martensite forms at dilutions of the LAS base metal with Alloy 625 filler metal that reduce the local A1 temperature below the PWHT temperature [5]. Carbon migration from the LAS forging towards the Alloy 625 butter weld during PWHT, caused by a steep gradient of the chemical potential across the dissimilar metal interface, results in carbide precipitation leading to local embrittlement [6–8]. Multiple authors have examined the effect of PWHT on the dissimilar interface microstructure and HAC cracking susceptibility of Alloy 625 butter welds on 8630 and F22 steel forgings [8–15].

The microstructure of the dissimilar interface between high strength steel forgings and Alloy 625 weld metal contains complex features that have been subjected to extensive investigation [6–8,11–13,16–19]. The compositional transition from steel base metal to diluted weld metal occurs over what has been called the partially mixed zone (PMZ) [6,11]. Due to a combination of low solidification rate and steep temperature gradient, a planar solidification zone forms at the interface between the steel coarse grained heat affected zone (CGHAZ) and the Alloy 625 weld metal. The planar growth region typically appears white after etching and therefore has also been referred to as a “featureless zone” [11] or “white etching region” [16]. It is also common to observe a thin band of martensite between the steel CGHAZ and the planar growth region [8]. The planar growth region has been found to have a face centered cubic microstructure [6,7,11,19]. The planar solidification breaks down into cellular or cellular dendritic solidification at a short distance from the fusion boundary.

Another distinctive feature of the dissimilar interface are the zones of macrosegregation, located mainly at interpass positions along the

* Corresponding author.
E-mail address: buntain.5@osu.edu (R. Buntain).

https://doi.org/10.1016/j.matchar.2020.110638
Received 5 November 2019; Received in revised form 29 April 2020; Accepted 11 September 2020
Available online 20 September 2020

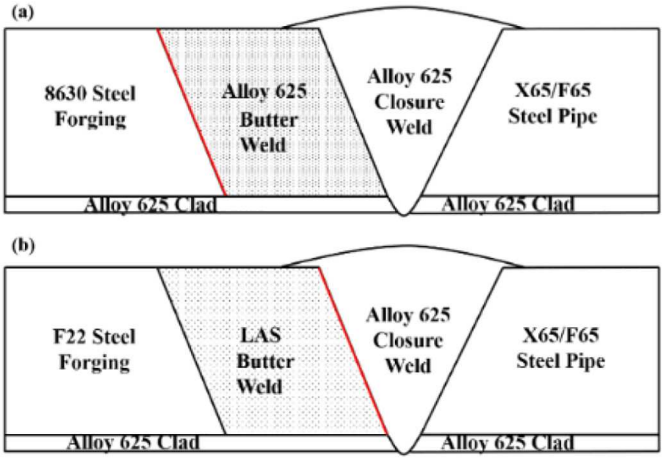

Fig. 1. Schematic of (a) traditional Alloy 625 butter weld on 8630 steel and (b) alternative LAS butter weld on F22 steel.

fusion boundary, which are frequently referred to as weld metal 'swirls' [5,7,11,18,19]. These features were also found to form at mid bead positions. A mechanism for macrosegregation in dissimilar welds between higher melting temperature base metals and lower melting welding consumables was proposed by Kou and Yang [20]. During welding, convection currents can sweep liquid base metal into the weld pool, where it is quickly cooled below its liquidus temperature and begins to solidify before complete mixing with the weld metal. The resulting macrosegregation zones, or swirls, typically contain 'peninsulas' or 'islands' with varying levels of dilution. The swirls in dissimilar welds of high strength steels with Alloy 625 filler metal typically contain martensitic constituents due to the increased hardenability resulting from enrichment with nickel and chromium [11,16].

To mitigate the HAC problem at the high strength steel forging/Alloy 625 interface, the oil and gas industry has explored replacing the Alloy 625 butter welds with those made of low alloy steel (LAS) filler metal [1], Fig. 1b. The high strength steel forging/LAS butter weld interface was intended to limit carbon migration and brittle carbide precipitation during onshore PWHT. After PWHT, the high strength steel forging/LAS butter weld assembly is joined to a low alloy steel pipe using Alloy 625 filler metal for the closure weld. However, the closure weld generates two dissimilar interfaces, LAS butter weld/Alloy 625 and LAS pipe/Alloy 625, which in the as-welded condition could potentially be susceptible to HAC [5].

In contrast with the extensive research performed on high strength steel forging/Alloy 625 butter weld interfaces, the microstructure and HAC susceptibility of the interfaces in Alloy 625 closure welds between LAS butter welds and low alloy steel pipes are still under investigation. The objective of this work is to characterize the microstructure along the dissimilar interfaces of an Alloy 625 closure weld between a LAS butter weld and F65 steel pipe in the as-welded condition. The formation mechanisms of the various microstructural features is also investigated. Special attention is paid to weld metal swirls and related microstructural constituents that are potentially susceptible to HAC.

2. Materials and procedures

A cross section of a girth weld between LAS butter weld and F65 steel pipe subjected to metallurgical characterization in the as-welded condition is shown in Fig. 2. The chemical compositions of the base metals and welding filler metals used in this dissimilar metal weld (DMW) are listed in Table 1. All compositions were taken from the mockup after welding using optical emission spectroscopy (OES). The Alloy 625 composition shown in Table 1 was taken from the diluted fusion zone after welding.

One side of the F22 pipe forging was overlaid (buttered) with a low alloy steel (LAS) welding consumable using a submerged arc welding (SAW) process. This weld assembly was internally clad with Alloy 625 filler metal using gas tungsten arc welding (GTAW) process and subjected to a stress relief post weld heat treatment (PWHT) for 6.5 h at 638 °C. The LAS butter layer was then joined to the F65 pipe with a narrow groove closure weld using a hot wire GTAW (HW-GTAW) process and Alloy 625 filler metal. The narrow groove weld was not subjected to PWHT after the closure welding procedure. The hot wire GTAW processes parameters are summarized in Table 2.

Samples for metallurgical characterization were prepared by mounting in Bakelite and grinding with 240, 320, 600 and 800 grit Si−C abrasive papers. Final polishing was performed using 9, 6 and 1 μm diamond paste followed by vibratory polishing using 0.05 μm colloidal silica. Initial etching in 2% Nital revealed the steel base metal microstructure. The weld metal microstructure was revealed by electrolytic etching in 10% Chromic acid at 5.0 V for 5 s. Light optical microscopy (LOM) was performed using an Olympus GX51 optical microscope. Scanning electron microscopy was performed using a FEI Apreo FEG microscope. Energy dispersive X-ray spectroscopy EDS maps were performed using an accelerating voltage of 20 kV, 1 μm step size and a 0.2 s dwell time. EDS line scans were performed at an accelerating voltage of 25 kV, 0.2 um step size and dwell time of 0.2 s. Electron backscattered diffraction (EBSD) was performed at 30 kV using a current of 3.2 nA.

Nanoindentation testing was performed at interpass positions using a MTS Nanoindentator XP with a Berkovich tip. All nanoindentation testing was performed under load control with maximum load of 3gf, 20 nm/s approach velocity, 35 s dwell time, and minimum spacing between indents of 15 μm.

Transmission electron microscopy (TEM) was performed on samples after nanoindentation. A platinum cap was deposited onto the sample prior to focused ion beam (FIB) milling. The FIB milling was performed using a FEI Helios 600 FIB. TEM images were taken on a FEI Titan G2 60–300 S/TEM microscope.

Thermodynamic simulations were performed using ThermoCalc™ software. The Scheil-Gulliver module was used to calculate non equilibrium liquidus and solidus temperatures. The simulations included the elements Fe, C, Ni, Cr, Mo, Mn and Nb with C assigned as a fast diffusing element. All simulations were ended when the fraction of solid reached 0.98. Semi quantitative EDS results were obtained with EDAX TEAM software using the eZAF algorithm. The EDS line scans for Fe, Ni, Cr, Mo and Mn were used as the input composition for the Scheil-Gulliver calculations. Due to the limitations of semi-quantitative EDS results, the C and Nb content had to be estimated using dilution calculations. The carbon content was calculated by multiplying the actual steel base metal carbon content with the dilution calculation as shown below:

$$\left(\frac{EDS\ Wt.\ \%Fe}{Average\ EDS\ Wt.\ \%Fe\ of\ BM}\right) * C\ content\ of\ base\ metal$$

The Nb composition was estimated in a similar manner using the average Ni content of the fusion zone Alloy 625 as shown below:

$$\left(\frac{EDS\ Wt.\ \%Ni}{Average\ EDS\ Wt.\ \%Ni\ of\ FM}\right) * Nb\ content\ of\ filler\ metal$$

3. Terminology definition

A common set of terminology that defines the microstructural features in the transition zone of dissimilar metal welds has not been established yet. Numerous authors have used the term 'partially mixed zone' (PMZ) to broadly describe the entire compositional gradient spanning the region from the unmelted steel base metal to the homogenously diluted fusion zone [6,10,19,21]. Local regions with a

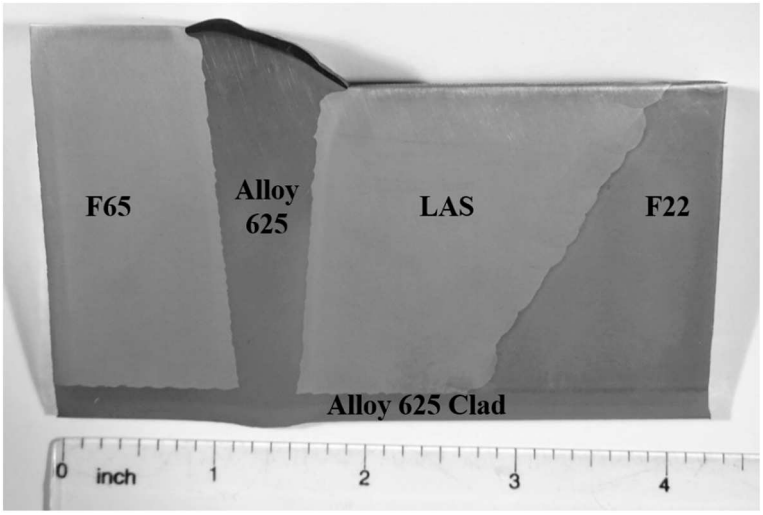

Fig. 2. Macro section of the characterized dissimilar metal weld.

composition resulting from incomplete mixing of base metal with Alloy 625 weld metal, were also defined as PMZs [18]. Furthermore, the PMZ was classified as having a continuous or discontinuous morphology [12]. The term 'continuous PMZ' was used to describe the interface that lacked local regions of macrosegregation. Fusion boundaries containing areas of macrosegregation, typically found at both mid-bead and bead overlap locations, were defined as 'discontinuous PMZs'. However, it is not clear if the term 'discontinuous PMZ' describes only the local and distinct macrosegregation feature or if it describes the entire compositional transition region which also spans both sides of the macrosegregation feature.

The term 'swirl' has commonly been used to describe the microstructural features observed at bead overlap positions. The swirls are protrusions of base metal that have been swept into the weld without significant mixing with the weld metal. These could also be called "peninsulas" or "islands" when using the terminology established by Kou and Yang [20] because they are most likely formed via a macrosegregation mechanism involving partial mixing of liquid base metal that is quickly cooled below its liquidus temperature. Thus, a zone of macrosegregation found at bead overlap positions could be described as 'swirl', 'peninsula', or 'discontinuous PMZ'.

In this paper swirls were found to be comprised of multiple microstructural features and will therefore be described using separate and distinct terminology for each feature. The term peninsula will be used to define regions of base metal that have been swept into the weld metal without significant mixing. The peninsulas will be shown to have a composition similar to the steel base metal, with a small increase in Ni and Cr content. Local regions that display a larger extent of partial mixing between the base and filler metal will be referred to as partially mixed zones using the acronym PMXZ. Thus, a PMXZ is considered to be a distinct local feature that formed due to literal partial mixing rather than the entire compositional transition region. The PMXZs will be shown to have a composition similar to the base metal, but with higher levels of alloying elements, mostly Ni and Cr, as compared to the peninsulas. The acronym PMXZ also helps differentiate the term 'partially mixed zone' from the 'partially melted zone' defined by Savage [22], which also uses the acronym PMZ. The term swirl will be used in a more general manner to describe the multiple microstructural features observed at the interpass positions. Thus, a swirl can contain multiple peninsulas, PMXZs, planar and cellular growth regions.

4. Results

A low magnification view of the fusion zone in the investigated closure weld is shown in Fig. 3. The LAS butter weld exhibited the typical microstructure of a multipass SAW weld deposit, containing large elongated columnar grains that are observable at low magnification. The F65 base metal was a forged pipe and contained a finer wrought microstructure that is not distinguishable at the low magnification shown in Fig. 3. The fusion boundary displayed a repetitive morphology that alternated between mid-bead and interpass positions. The white etched constituents observed at the fusion boundary are regions of planar growth. These regions are typically thinner at mid-bead positions and extend into the weld metal at interpass locations as part of weld metal swirls. This paper is focused on metallurgical characterization of the interpass swirls, while the mid-bead microstructures will be a subject of a separate publication.

4.1. Swirls morphology overview

The weld metal swirls, found at the interpass positions in the investigated weld, consisted of partially mixed base metal swept into the weld pool which solidified prior to complete mixing. An example of a swirl morphology is shown in Fig. 4.

This particular swirl contains two iron-rich peninsulas that are surrounded by PMXZs, planar and cellular growth regions. The iron-rich peninsulas can be distinguished from the PMXZs based on dilution level and response to etching in 2% nital. The steel-rich peninsulas respond to etching similarly as the F65 base metal and the PMXZs have a solid grey appearance after etching. Regions of planar growth that break into cellular growth can be seen surrounding the PMXZs. As shown in the phase map of Fig. 4d, the iron-rich peninsulas and PMXZs

Table 1
Materials chemical compositions determined using optical emission spectroscopy, wt%.

Material	Fe	C	Ni	Cr	Mo	Mn	Nb	Ti	Si	P	S
LAS butter	Bal.	0.06	0.92	0.16	0.58	1.41	< 0.01	< 0.01	0.21	0.014	0.002
F65 steel	Bal.	0.10	0.52	0.22	0.27	1.17	0.03	< 0.01	0.22	0.006	0.002
Alloy 625	4.59	0.04	60.7	21.4	8.74	0.69	3.24	0.08	0.41	< 0.005	0.004

Table 2
Weld parameters used for the narrow groove HW-GTAW procedure.

Voltage (V)	Current (A)	Wire feed speed (m/min)	Travel speed (mm/min)	Minimum preheat/ Interpass temperature (°C)	Hot wire voltage (V)	Hot wire current (A)	Filler wire diameter (mm)
10	260	1.78	88.9	200	2.0	60–70	1.14

have a body centered cubic (BCC) crystal structure. Note that EBSD is unable to distinguish BCC crystal structures from body centered tetragonal (BCT) crystal structures therefore any BCT martensite within the PMXZs would index as BCC. The white planar and cellular growth regions, and weld metal displayed a face centered cubic (FCC) crystal structure. A BCC 'island" that is not attached to the main swirl can be seen below the steel-rich peninsula.

The IPF map in Fig. 4c shows one large FCC grain surrounding the steel-rich peninsulas and PMXZs. This FCC grain is composed of the planar and cellular growth regions surrounding PMXZs, and of dendritic weld metal. The IPF map also shows that the large FCC grain interfaces a series of smaller FCC grains, with planar and cellular structure, nucleating from the CGHAZ and from the PMXZ of another swirl. That interface delineates two opposite solidification fronts originating from the swirl and the CGHAZ.

4.2. Microstructure of F65 / Alloy 625 interface swirl

A light optical micrograph along with EDS maps of a weld metal swirl at the F65/Alloy 625 interface is shown in Fig. 5. This swirl is composed of three steel-rich peninsulas surrounded by PMXZs and white etching planar and cellular growth regions. The EDS maps show that the peninsulas have iron contents similar to the base metal. The PMXZs, planar and cellular regions are enriched in nickel and chromium to levels greater than the steel base metal but lower than the weld metal composition. Niobium-rich particles were found within the PMXZs, planar, and cellular regions, Fig. 5f.

EBSD scans of the swirl discussed above are shown in Fig. 6. Both the iron-rich peninsulas and the PMXZs have a BCC structure, Fig. 6c. The planar and cellular growth regions displayed a FCC crystal structure. A narrow band of austenite was also found directly at the fusion boundary. The image quality map shown in Fig. 6a revealed that the iron-rich peninsulas and the planar growth regions have a higher index quality than the PMXZs. The low index quality regions appear to have a much finer microstructure in the IPF map, Fig. 6b. Similar to the swirl shown in Fig. 4c, one large FCC grain surrounds the outermost iron-rich peninsula. Planar growth regions nucleating from the outermost and innermost peninsulas interface a series of enclosed cellular grains, showing evidence of opposite solidification directions.

A nanoindentation map of the same swirl is shown in Fig. 7. The level of alloying additions can be approximated by the contrast provided by the backscattered electron image, with the regions containing higher levels of nickel and chromium having a lighter contrast. The highest hardness was observed in the PMXZ directly adjacent to the fusion boundary. In general, the nickel and chromium enriched PMXZs had the highest hardness. The hardness of the iron-rich peninsulas was similar or slightly higher than the F65 base metal, but significantly lower than the PMXZs' hardness. The higher magnification SEM image in Fig. 7b shows that the regions of high hardness had a lath-like microstructure. The base metal showed an equiaxed microstructure.

An EDS traverse across the same swirl is shown in Fig. 8, together with ThermoCalc predicted liquidus and solidus temperatures. The EDS traverse across row 5 reveals an alternating composition profile between the three iron-rich peninsulas and the three nickel and chromium-rich PMXZs. The amount of Ni and Cr in the PMXZs increased as the location moved from the fusion boundary towards the fusion zone. Although not shown in Fig. 8, EDS line scans were also performed across rows 4, 5, and 6. Table 3 summarizes the compositions and solidification temperature range of the Fe-rich peninsulas and the PMXZs for rows 4–6. The iron-rich peninsulas had similar compositions to the F65 base metal but with slightly higher nickel and chromium contents. The nickel and chromium content of the PMXZs was higher compared to the peninsulas and lower compared to the weld metal. The amount of nickel in the PMXZs and peninsulas increased as the location moved towards the bottom of the swirl.

The predicted liquidus, solidus, and solidification temperature ranges (STR) of the peninsulas and PMXZs, along with the base and filler metals are also shown in Table 3. The predicted base metal solidus temperature was significantly higher than the weld metal liquidus temperatures. The peninsulas had lower solidus temperatures and wider STR compared to the base metal, and were predicted to complete solidification approximately 30 to 40 °C above the weld metal liquidus temperature. The PMXZs had a wider STR and 90 to 150 °C lower solidus temperature compared to the peninsulas. The PMXZs were predicted to complete solidification at about 130 °C above the weld metal solidus temperature, indicting an overlap in STR between the PMXZs and weld metal.

TEM was performed on a region spanning from the F65 base metal to the nickel and chromium-rich PMXZ. The location of the FIB foil extraction is shown by the black line in Fig. 8. The F65 base metal,

Fig. 3. Low magnification optical micrograph of the LAS butter weld (left) joined to the F65 steel pipe (right) using Alloy 625 filler wire.

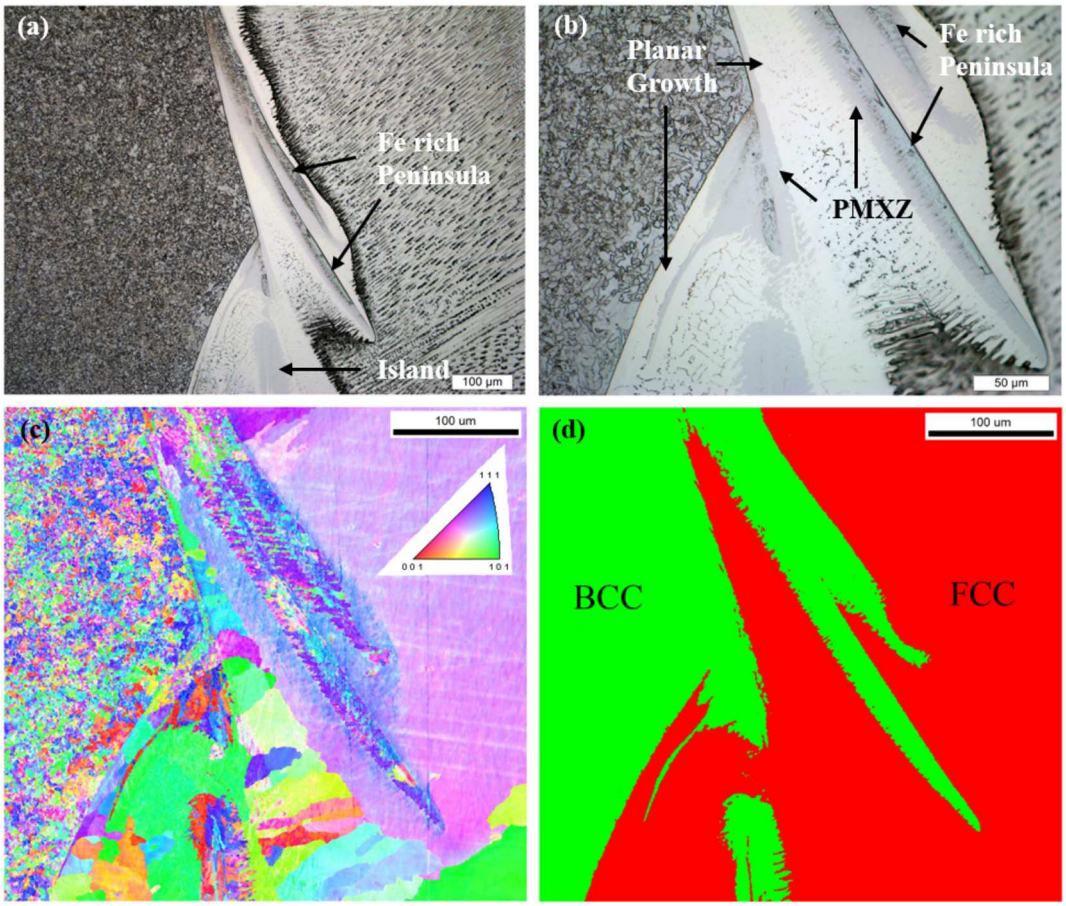

Fig. 4. Optical micrograph of F65/Alloy 625 inter pass swirl (a,b), EBSD IPF map (c) and phase map (d).

shown on the left side of the foil in Fig. 9b, had an equiaxed microstructure. The microstructure of the PMXZ, shown in Fig. 9c and d, was comprised of lath martensite.

4.3. Microstructure of LAS butter weld / Alloy 625 interface swirl

An interpass swirl located along the LAS butter weld/Alloy 625 interface along with EDS maps is shown in Fig. 10. The portion of the swirl located slightly above the interpass position was subjected to metallurgical characterization. The optical micrographs in Fig. 10a and b show a grey etched PMXZ located between an iron-rich peninsula and the LAS base metal. A planar growth region nucleated from the peninsula and the PMXZ breaks into cellular growth towards the weld metal. The distinction between the iron-rich peninsula and the PMXZ is

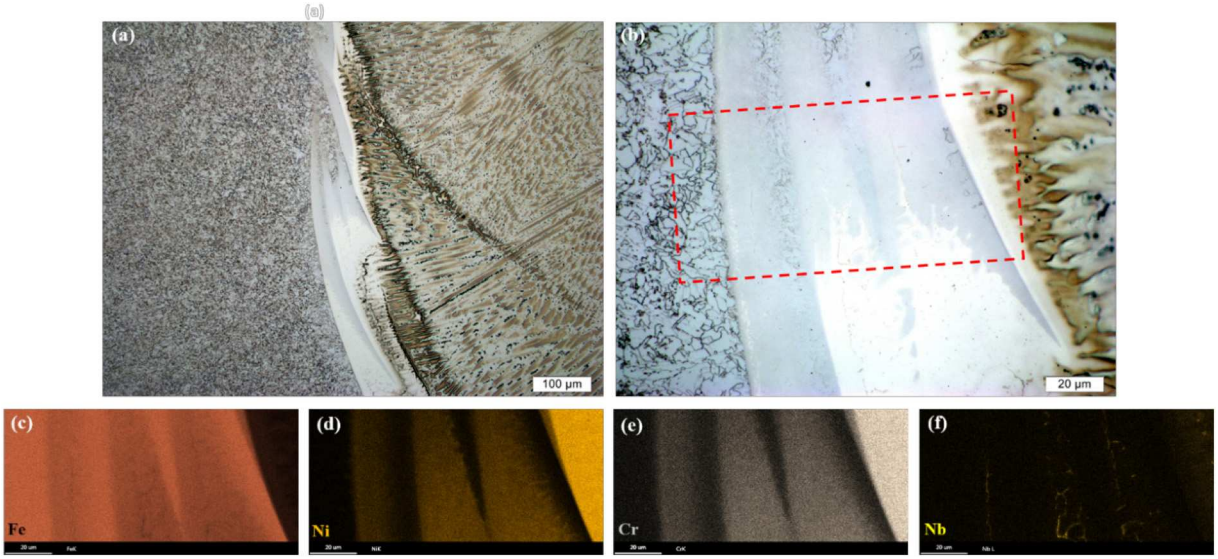

Fig. 5. Optical micrographs (a,b) of a F65/Alloy 625 interpass swirl along with EDS maps showing Fe (c), Ni (d), Cr (e) and Nb (f) distributions within the area outlined in red. (For interpretation of the references to colour in this figure legend, the reader is referred to the web version of this article.)

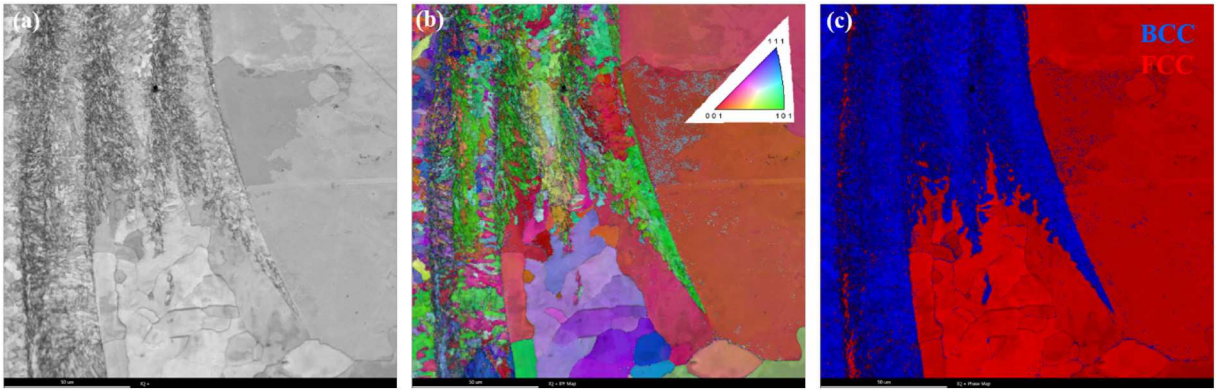

Fig. 6. EBSD image quality map (a), IPF map (b) and phase map (c) of F65/Alloy 625 swirl shown in Fig. 5.

not obvious when etched in 2% nital, but is more distinguishable through the EDS maps in Fig. 10c through 10f. The peninsula is enriched in iron and contains less chromium and nickel than the PMXZ, which borders the base metal.

EBSD scans of the same LAS butter weld/Alloy 625 swirl are shown in Fig. 11. The image quality and IPF map revealed the PMXZ had a finer microstructure with a low index quality compared to the iron-rich peninsula. Both the PMXZ and iron-rich peninsula had a BCC crystal structure while the planar and cellular growth regions along with the weld metal had a FCC crystal structure. The PMXZ contained small amounts of retained austenite. Similar to Fig. 4 and Fig. 6, one large FCC grain, containing weld metal and the swirl's planar and cellular zones, borders the iron-rich peninsula and the PMXZ.

A nanoindentation map of the LAS butter weld/Alloy 625 swirl is shown in Fig. 12. Similar to the F65/Alloy 625 swirl shown in Fig. 7, the highest hardness was observed in the PMXZ. The iron-rich peninsula had a higher hardness than the LAS base metal, but lower than the PMXZ. The SEM backscattered image in Fig. 12b shows a finer, lath like microstructure in the PMXZ which is most likely martensite.

An EDS traverse across the same LAS butter weld/Alloy 625 swirl, along with the ThermoCalc predicted liquidus and solidus temperatures, is shown in Fig. 13. The content of main alloying elements in the peninsula, PMXZ, LAS butter, and Alloy 625 weld metal, together with their liquidus and solidus temperatures, and STRs are summarized in Table 4. The EDS traverse confirms that the peninsula has lower iron and higher nickel and chromium contents than the LAS butter weld. The PMXZ has lower iron and higher nickel and chromium content compared to the peninsula. The LAS butter weld has a STR of 74 °C and solidus temperature 58 °C above the Alloy 625 weld metal liquidus. The peninsula has a solidus temperature almost equal to the weld metal liquidus and the PMXZ solidifies at 90 °C above the weld metal solidus.

5. Discussion

5.1. Narrow groove swirl morphology

Previous studies on the dissimilar fusion boundary microstructure of high strength steel/Alloy 625 joints have examined both bead on plate [10] and butter welds [5,7,12]. Such welds are typically performed using a hot wire GTAW process in the flat horizontal position where the welding arc is orientated normal to the steel substrate. Published research on such butter welds describes comparatively short interpass swirls, typically containing a single iron-rich peninsula and one PMXZ enclosed between the peninsula and the base metal. Such swirl morphology can be related to a smaller weld pool volume and more extensive pool convection generated by the butter weld procedure.

The narrow groove geometry in closure welds, where the welding arc contacts the groove surface at a sharp angle, requires higher heat inputs to ensure full penetration of the base metal. The resulting weld pool is larger and more constrained, generating conditions for melting larger amounts of base metal that is swept into and partially mixed with the weld. Thus, large areas of macro-segregation are formed at the dissimilar interface interpass positions in the form of swirls composed of multiple iron-rich peninsulas and PMXZs. As shown in Figs. 3, 4a, 5a, and 10a, these swirls can extend over one millimeter in length and a hundred micrometers in width. The presence of multiple iron-rich peninsulas and PMXZs within a single swirl appears to be a unique feature of narrow groove closure welding.

As demonstrated in the results section, the weld metal swirls in both interfaces contained multiple microstructural features due to varying

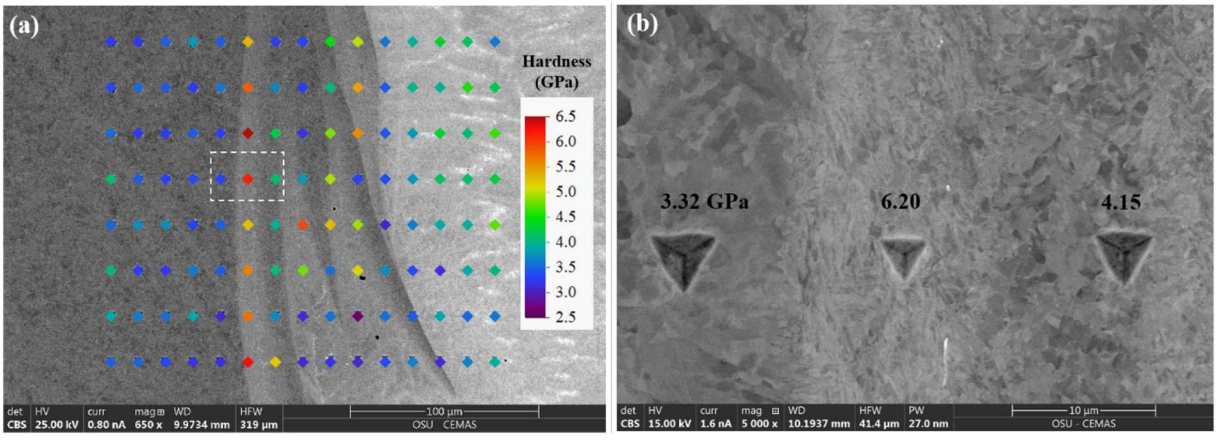

Fig. 7. Nanoindentation map (a) of F65/Alloy 625 swirl along with backscattered SEM image (b) of area highlighted in white.

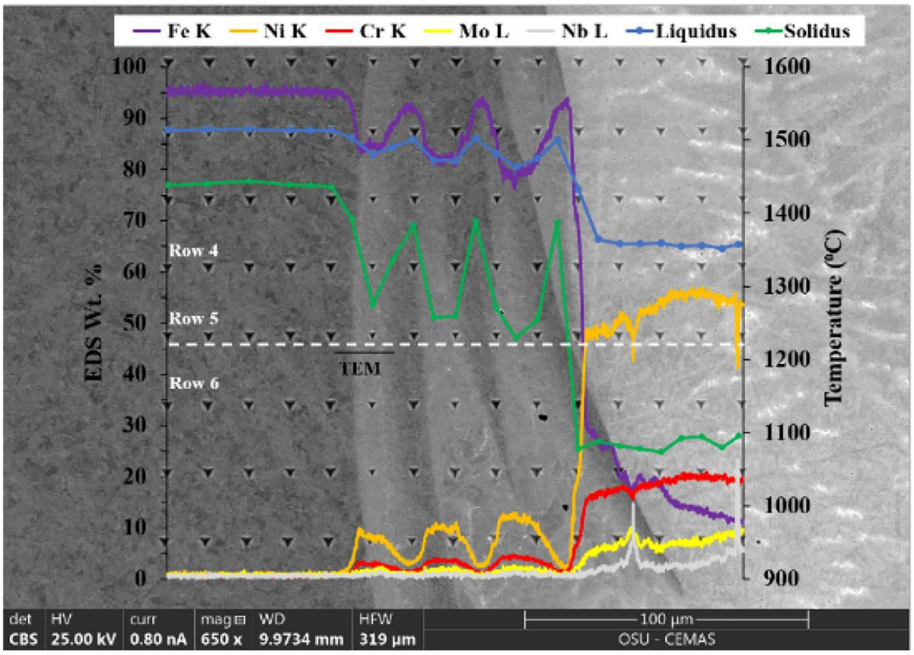

Fig. 8. Backscatter SEM image of F65/Alloy 625 swirl overlaid with row 5 EDS traverse (white line) and ThermoCalc predicted solidus and liquidus temperatures.

solidification conditions and degree of partial mixing. Therefore, the term swirl is used in this paper to more broadly describe the entire interpass morphology comprised of multiple iron-rich peninsulas, PMXZs, and surrounding planar and cellular growth regions.

5.2. Swirl formation mechanism

The mechanism of swirl formation in the investigated dissimilar closure weld is analyzed below following the macrosegregation mechanism proposed by Kou and Yang [20,23] and the sequence of solidification events in the swirl components shown in Figs. 6 and 13 and in Tables 3 and 4. As shown in Tables 3 and 4, the F65 steel base metal and the LAS butter weld have narrow STRs and solidus temperatures about 80 °C higher than the liquidus temperature of Alloy 625 filler metal. Such differences in the solidification behavior, complemented by the intensive convection within the weld pool, create conditions for non-uniform mixing of the liquid steel base metal swept into the pool. The resulting sharp gradients in the composition and solidification events (Figs. 8, 13) lead to formation of swirls with the complex morphology shown in Figs. 3, 4, 5, and 10.

The least mixed base metal, containing small amounts of nickel and chromium (Tables 3, 4), solidifies first in a narrow STR above the weld metal liquidus temperature, forming multiple iron-rich peninsulas (Figs. 4, 5, 10) and islands (Fig. 4). The enrichment in nickel and chromium of the peninsulas could be due to a small degree of partial mixing and/or high temperature diffusion from the surrounding liquid.

The iron-rich peninsulas are separated from each other, and from the base metal, by PMXZs with a higher degree of mixing, containing up to 12% Ni and 4% Cr. Possible mechanism of PMXZ formation involves a stagnant layer of liquid trapped between the solidifying peninsulas and base metal, with limited access to stirring and mixing with the bulk weld pool. The PMXZs begin to solidify relatively quickly, approximately 20–40 °C degrees below the peninsulas' liquidus temperature, thus adding a temporal restriction to the physical restriction from complete mixing with the bulk weld pool. The increasing gradients of chromium and nickel contents from locations closer to the fusion boundary and higher up in the swirl towards the fusion zone (Table 3), evidence the role of restricted mixing in the formation of PMXZs.

The solidification sequence in the swirls is led by the iron-rich peninsula solidifying about 80 °C above the bulk weld pool liquidus temperature, followed by the PMXZs solidifying 130 to 200 °C above the weld pool solidus. This is followed by planar and cellular growth regions nucleating from the PMXZs. Due to their level of alloying with nickel and chromium, the PMXZs solidify as austenite and remain in austenitic state on cooling before transforming to martensite, thus providing FCC substrate for epitaxial nucleation of the planar and cellular zones, Figs. 4d and 6c.

The optical micrograph in Fig. 4b shows white etching planar and cellular solidification morphologies formed between two PMXZs. The PMXZ on the left nucleates from the base metal and from a peninsula directly connected to the base metal. The PMXZ on the right nucleates from a longer peninsula located closer to the bulk weld pool. Both PMXZs provide substrates for epitaxial nucleation and growth of planar and cellular morphologies with opposite growth directions. These

Table 3
Summary table of EDS line scans and solidification temperature predictions.

Region	Row	Fe wt%	Ni wt%	Cr wt%	Liquidus (°C)	Solidus (°C)	STR (°C)
Peninsula	4	93.3	2.4	1.2	1507	1395	113
	5	92.5	2.9	1.5	1504	1396	108
	6	91.9	3.2	1.7	1502	1388	114
PMXZ	4	86.8	6.8	2.5	1486	1301	184
	5	81.9	10.1	3.6	1472	1264	209
	6	78.8	12.0	4.3	1464	1246	219
F65 BM	4–6	95.3	0.9	0.6	1514	1437	77
Alloy 625 filler metal	4–6	12.4	55.6	19.9	1355	1118	237

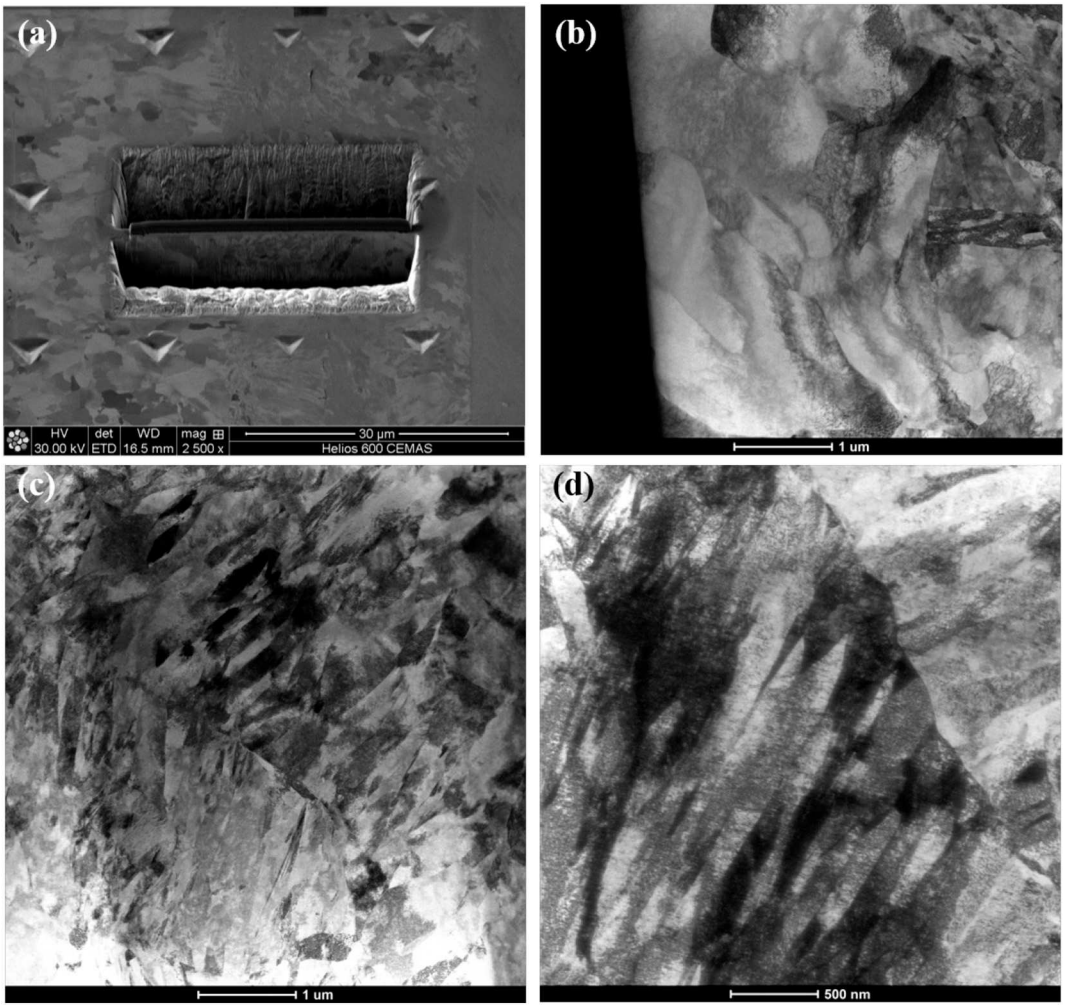

Fig. 9. TEM results from F65/Alloy 625 swirl showing FIB foil extraction (a), F65 base metal (b) and PMXZ microstructure (c, d).

opposite solidification fronts meet to form a solidification boundary within the swirl. This internal interface in the swirl morphology is shown in the IPF map of Fig. 4c. Evidence for opposite solidification fronts can be also found in the swirl shown in Fig. 6. Planar zones nucleate and grow in opposite directions between the PMXZs of the inner and outermost iron-rich peninsula. The planar zones break into cellular grains with similar orientation (Fig. 6b), generating two solidification interfaces with the cellular morphologies and multiple grain boundaries between the cellular grains.

The solidified iron-rich peninsulas that are in direct contact with the weld pool could serve as sites for epitaxial nucleation of planar and cellular growth solidification morphologies within the weld metal. Evidence for such behavior is presented by EBSD scans in Figs. 4c and 6b, which show one large FCC grain surrounding the outermost peninsulas and the related PMXZs. Multiple examples of a single large FCC grain surrounding the outer swirl peninsulas have been found in the examined closure weld. Similar examples have also been reported for swirls in butter welds [7].

The morphological features generated by the above described swirl formation mechanism, including the swirl-internal planar/cellular and cellular/cellular solidification interfaces, the cellular grain boundaries, and the large FCC grains, are similar to those found in dissimilar butter welds [7].

5.3. Swirl microstructure

Due to the limited and non-uniform mixing during solidification, and the resulting sharp compositional gradients, the swirl components exhibit a variety of microstructural constituents in their final microstructure. Although enriched in nickel and chromium, as compared to the base metal CGHAZ, the iron-rich peninsulas exhibit similar equiaxed microstructure. Such similarities are shown in backscattered images in Figs. 7b and 12b, in the image quality maps in Figs. 6a and 11a. However, the hardness in the more diluted regions of the peninsulas is higher than the F65 steel and LAS coarse-grained HAZs, Figs. 7a and 12a. The peninsulas' hardness is a product of their higher hardenability and potential bainitic and/or martensitic transformation on cooling, followed by tempering generated from subsequent weld passes. The effect of potential carbon depletion on the peninsulas hardness needs to be also considered. Carbon migration from the peninsulas towards the surrounding liquid, enriched in Alloy 625, would be driven by the gradient of chemical potential at the solid/liquid interface.

The PMXZs exhibited significantly higher hardness compared to the surrounding base metal coarse-grained HAZ, iron-rich peninsula, and weld metal, Figs. 7a and 12a. This can be attributed to formation of martensite due to the higher alloying content and hardenability of the PMXZs, and potential carbon enrichment from the neighboring base metal HAZ and iron-rich peninsula. Indirect evidence of carbon migration towards the PMXZs is provided by the fact that the hardest PMXZs are located next to the base metal and border narrow carbide-free regions in HAZ, as shown in Figs. 5 and 10. Carbon depletion of the steel HAZ and accumulation in the compositional transition zone during PWHT of dissimilar metal welds with Alloy 625 filler metal has been

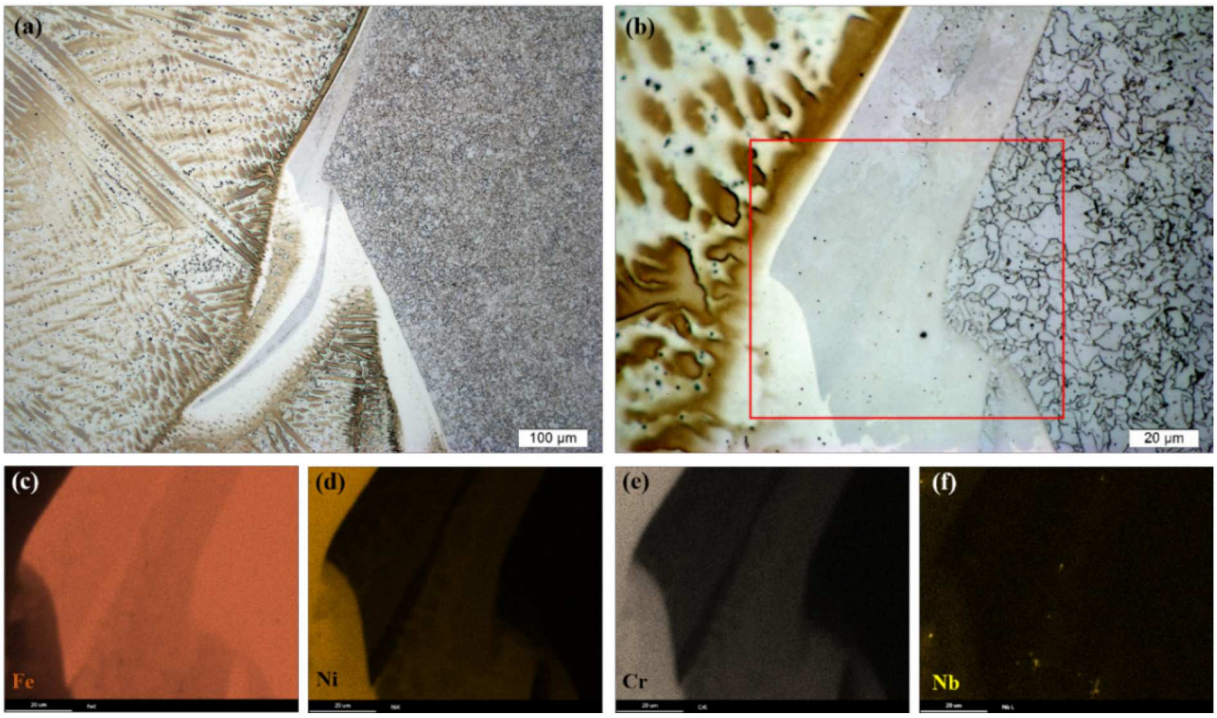

Fig. 10. Optical micrographs (a,b) of LAS / Alloy 625 swirl along with EDS maps showing Fe (c), Ni (d), Cr (e) and Nb (f) distributions of the area outline in red. (For interpretation of the references to colour in this figure legend, the reader is referred to the web version of this article.)

broadly investigated and proven [6,7,19]. A recent study has proven that during welding, carbon migration of significant extent can occur across the dissimilar interface due to the sharp chemical potential gradient created by the composition of Alloy 625 [27].

A lath martensitic microstructure within the hardest PMXZ shown in Fig. 7a was confirmed by the TEM images shown in Fig. 9. The lath microstructure in the same PMXZ and the one shown in Fig. 12a can be observed in Figs. 7b and 12b as well. The EBSD image quality maps in Figs. 6a and 11a show low image quality of the PMXZs. EBSD is unable to distinguish the crystal structures of BCC ferrite and BCT martensite. However, it has been shown that due to higher lattice distortions, martensitic microstructures typically have lower EBSD image quality values than ferritic microstructures [23–25].

The wide range of dilution levels combined with possible tempering from the multipass weld procedure could result in both untempered and tempered martensite, and bainitic microstructures within one weld metal swirl. It has to be noted that the probability of bead tempering in the PMXZs is lower than in the iron-rich peninsula. The higher nickel content of the PMXZs would reduce their Ac1 and Ac3 temperatures, increasing the probability for re-austenitization and reformation of fresh martensite during multipass welding.

The hard untempered martensitic constituent, which was identified in PMXZs, could be susceptible to hydrogen assisted cracking (HAC). Hydrogen can reach such PMXZs through the CGHAZ and the iron-rich peninsula, which would provide fast diffusion paths in case the LAS pipe or butter weld are directly exposed to the service environment. Due to the steep composition and microstructure gradients in the dissimilar transition zone, and the resulting property gradients, the large swirls that form in narrow groove closure welds would act as internal stress concentrators. Thus, hydrogen assisted cracks could potentially nucleate in the martensitic PMXZs if a critical combination of stress intensity and hydrogen concentration is reached.

6. Summary and conclusions

The results of this study show that the formation of swirls in closure welds of low alloy steels pipes with Alloy 625 filler metal is controlled by the differences in the materials composition and solidification behavior, and by the weld pool convection related to the weld geometry and the welding process. Incomplete and non-uniform mixing results in a sequence of solidification events that produce microstructurally distinctive swirl components and swirl internal interfaces. A summary of the formation mechanism and microstructural features of the swirls in the examined narrow groove closure weld between low alloy steel (LAS) butter weld and F65 steel pipe with Alloy 625 filler metal, which was in the as-welded condition, is presented below.

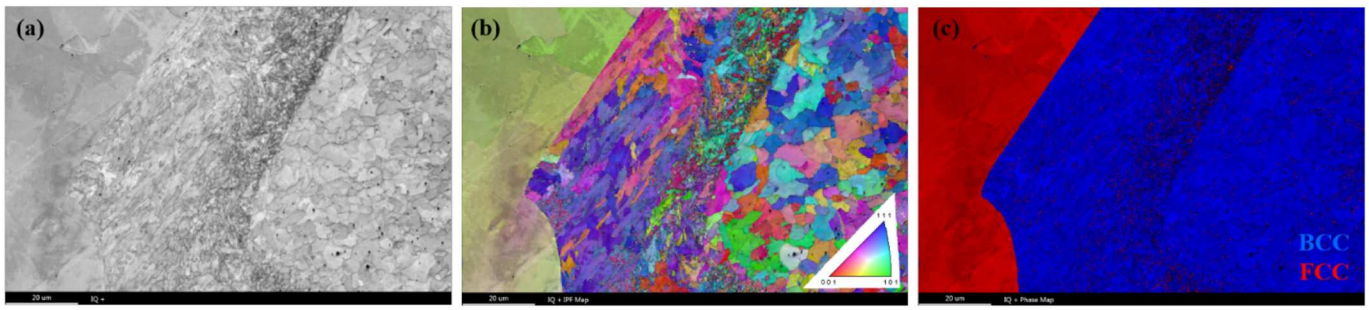

Fig. 11. EBSD scan of LAS / Alloy 625 swirl showing image quality map (a), IPF map (b) and phase map (c).

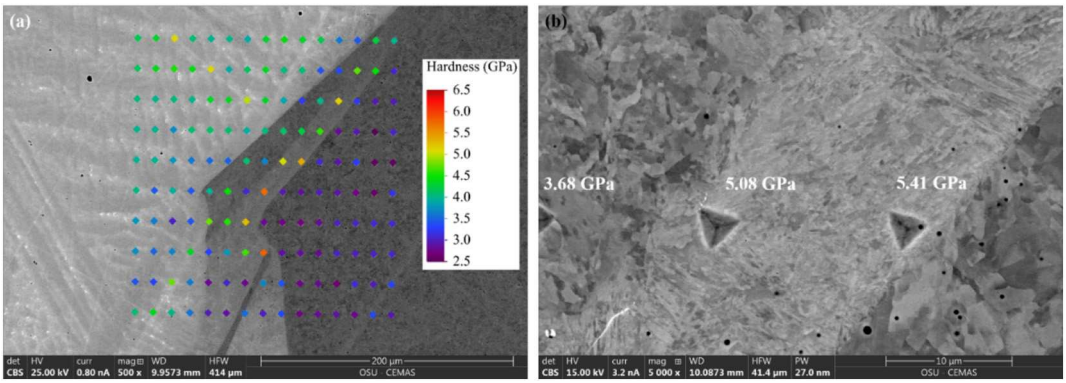

Fig. 12. Nanoindentation map (a) of LAS / Alloy 625 swirl and with SEM backscattered image (b) of area highlighted in white.

- The weld metal swirls are comprised of multiple iron-rich peninsulas alternating with partially mixed zones (PMXZ), and include planar and cellular zones.
- The swirl components solidify in the above listed sequence with the peninsula and PMXZs providing substrates for epitaxial solidification of the planar and cellular zones.
- The planar and cellular zones have closer composition to the Alloy 625 weld metal and FCC structure. These can have opposite growth directions, resulting in solidification interfaces within the swirls.
- Large FCC grains nucleate epitaxially off the outermost swirl peninsula. These grains contain planar, cellular, and dendritic zones, and have similar composition to the weld metal.
- The iron-rich peninsulas have BCC crystal structure with equiaxed grain morphology that is similar to the base metal HAZ. The peninsulas' nickel and chromium content, and hardness are higher compared to the base metal HAZ.
- The PMXZs have higher nickel and chromium contents than the peninsulas, increased hardenability, and martensitic microstructure.
- The martensitic constituents present in the PMXZs could serve as nucleation cites for hydrogen assisted cracking (HAC).
- The swirl internal interfaces, originating from opposite solidification fronts, and the large FCC grains, nucleating from iron-rich peninsulas, could provide low energy paths for crack propagation.
- Compared to Alloy 625 butter welds on high strength steel substrates, the swirls in narrow gap closure welds contain similar microstructural features, but are significantly larger and have a branched morphology of multiple peninsula alternating with PMXZs.

The low alloy steel butter welds were developed to mitigate the detrimental effect of carbon migration and carbide precipitation during PWHT on the HAC susceptibility of Alloy 625 butter welds. However, the results of this study show that the swirls formed at the LAS butter weld/Alloy 625 and F65 steel/Alloys 625 interfaces in narrow groove closure welds, which are in the as-welded condition, contain microstructural constituents that could be susceptible to HAC. The HAC susceptibility of these interfaces is the subject of a separate study.

Data availability

The raw/processed data required to reproduce these findings cannot be shared at this time as the data also forms part of an ongoing study.

Declaration of Competing Interest

The authors declare that they have no known competing financial interests or personal relationships that could have appeared to

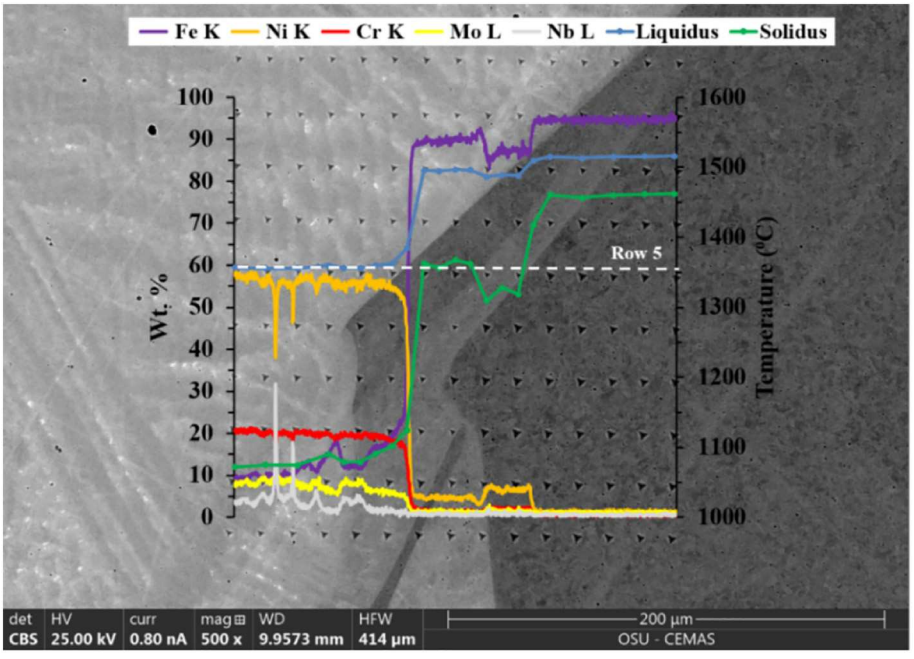

Fig. 13. Backscattered SEM image overlaid with EDS line scan across row 5 (white line) and ThermoCalc predicted liquidus and solidus temperatures.

Table 4
Summary of EDS compositions and solidification temperatures of LAS / Alloy 625 swirl.

Region	Row	Fe wt%	Ni wt%	Cr wt%	Liquidus (°C)	Solidus (°C)	STR (°C)
Peninsula	5	89.8	4.6	1.6	1496	1365	131
PMXZ	5	86.9	6.7	2.2	1487	1316	171
LAS BM	5	94.7	1.4	0.4	1514	1441	74
Alloy 625 filler metal	5	9.7	57.0	20.4	1356	1126	230

influence the work reported in this paper.

Acknowledgements

The authors would like to acknowledge the Manufacturing and Materials Joining Innovation Center (Ma^2JIC), made possible through an award (18-22144) from the National Science Foundation Industry University Cooperative Research Center program (IUCRC), for financial support. The SEM and TEM characterization work was performed at the Ohio State University Center for Electron Microscopy and Analysis (CEMAS).

The authors acknowledge the guidance and advice of Mr. Dean Hannam and Mr. Nash Ubale, formerly with Schlumberger, and of Dr. Clint Wildash and Mr. James Alban from Schlumberger.

References

[1] J.D. Burk, C.L. Ribardo, B.P. America, Thunder Horse – Materials , Welding and Corrosion Challenges and Solutions, Offshore Technol. Conf, 2010.
[2] L.M. Haldorsen, M. Dodge, G. Rorvik, K. Sotoudeh, Recent experiences with cracking of load bearing dissimilar metal welds on subsea production systems, Ocean, Offshore and Arctic Engineering, 2017, pp. 1–13.
[3] M.F. Gittos, K. Sotoudeh, S. Smith, H. Pisarski, G. Park, Failure of an AISI 8630-Mod low alloy steel to C-Mn steel dissimilar metal weld made using nickel alloy UNS N06625 welding consumables, Nace, 2015, pp. 1–18 no. 5500.
[4] P.E. Kvaale, G. Rorvik, T. Habrekke, Experience with qualification and use of stainless steels in subsea pipelines, Offshore Mechanics and Arctic Engineering, 2004.
[5] M.F. Dodge, The Effect of Heat Treatment on the Embrittlement of Dissimilar Welded Joints, University of Leicester, 2014.
[6] J.a. Fenske, I.M. Robertson, R. Ayer, M. Hukle, D. Lillig, B. Newbury, Microstructure and hydrogen-induced failure mechanisms in Fe and Ni alloy weldments, Metall. Mater. Trans. A Phys. Metall. Mater. Sci. 43 (9) (2012) 3011–3022.
[7] B.T. Alexandrov, J.C. Lippold, J.W. Sowards, A.T. Hope, D.R. Saltzmann, Fusion boundary microstructure evolution associated with embrittlement of Ni – base alloy overlays applied to carbon steel, Weld World 57 (2013) 39–53.
[8] M.F. Dodge, H.B. Dong, M. Milititsky, R.P. Barnett, V.F. Marques, M.F. Gittos, Environment – Induced Cracking in Weld Joints in Subsea Oil and Gas Systems – Part I, Ocean, Offshore and Arctic Engineering, 2012, pp. 1–8.
[9] M.F. Gittos, Resistance of dissimilar joints between steel and nickel alloys to hydrogen-assisted cracking, Nace, 2008, pp. 1–8 no. 3.
[10] V.C.M. Beaugrand, L.S. Smith, M.F. Gittos, Hydrogen embrittlement of 8630M / 625 subsea dissimilar joints: Factors that influence the performance, Proceedings of the 28th International Conference on Ocean, Offshore and Arctic Engineering, 2009, pp. 1–10.
[11] M.F. Beaugrand, C.M. Viviane, L.S. Smith, Gittos, Subsea dissimilar joints: failure mechanisms and opportunities for mitigation, Corrosion, 2009, pp. 1–12 no. 09305.
[12] J. Fenske, Microstructure and Hydrogen Induced Failure Mechanisms in Iron-Nickel Weldments, University of Illinois, 2010.
[13] C. Fink, B.T. Alexandrov, Effect of post-weld heat treatment on fusion boundary microstructure in dissimilar metal welds for subsea service, Mater. Test. 59 (6) (2017) 547–554.
[14] B. Alexandrov, J.M. Rodelas, S. Shi, J. Lippold, A new test for evaluation of susceptibility to hydrogen assisted cracking in dissimilar metal welds, NACE Int. (2012) 11.
[15] T. Dai, J.C. Lippold, The effect of postweld heat treatment on hydrogen-assisted cracking of 8630/Alloy 625 overlay, Weld. World 62 (3) (2018) 581–599.
[16] V. Olden, P.E. Kvaale, P.A. Simensen, S. Aaldstedt, J.K. Solberg, The effect of PWHT on the material properties and micro structure in Inconel 625 and Inconel 725 buttered joints, Proceedings of OMAE 2003, 2003, pp. 109–115.
[17] T. Dai, J. Lippold, Characterization of the Interface of an Alloy 625 overlay on steels using Nanoindentation, J. Mater. Eng. Perform. 27 (7) (2018) 3411–3418.
[18] T. Dai, J.C. Lippold, Tempering effect on the fusion boundary region of alloy 625 weld overlay on 8630 steel, Weld. World 62 (3) (2018) 535–550.
[19] M.F. Dodge, H.B. Dong, M.F. Gittos, T. Mobberley, Fusion zone micostructure associated with embrittlement of subsea dissimilar joints, OOAE 2014, 2014.
[20] S. Kou, Y.K. Yang, Fusion boundary macrosegregation in dissimilar-filler welds, Weld. J. 86 (10) (2007) 331–339.
[21] A. Bahrami, M. Gittos, H. Pisarski, P. Woollin, Assessing the integrity of subsea dissimilar joints to ensure safe operations, Offshore Technology Conference, 2010.
[22] W.F. Savage, E.F. Nippes, E.S. Szekeres, A study of weld Interface phenomena in a low alloy steel, Weld. J. 55 (9) (1976) 260–268.
[23] A.W. Wilson, G. Spanos, Application of orientation imaging microscopy to study phase transformations in steels, Mater. Charact. 46 (5) (2001) 407–418.
[24] P.T. Pinard, A. Schwedt, A. Ramazani, U. Prahl, S. Richter, Characterization of dual-phase steel microstructure by combined submicrometer EBSD and EPMA carbon measurements, Microsc. Microanal. 19 (4) (2013) 996–1006.
[25] A.J. DeArdo, C.I. Garcia, K. Cho, M. Hua, New method of characterizing and quantifying complex microstructures in steels, Mater. Manuf. Process. 25 (1–3) (2010) 33–40.